Doubly resonant surface-enhanced Raman scattering on gold nanorod decorated inverse opal photonic crystals

Le Dac Tuyen,[1,2] An Chi Liu,[1] Chia-Chi Huang,[3] Pei-Cheng Tsai,[1] Jian Hung Lin,[1] Chin-Wei Wu,[3] Lai-Kwan Chau,[3,6] Tzyy Schiuan Yang,[3] Le Quoc Minh,[4] Hung-Chih Kan,[1,7] and Chia Chen Hsu[1,5,*]

[1]*Department of Physics, National Chung Cheng University, Ming Hsiung, Chia Yi 621, Taiwan*
[2]*Department of Physics, Hanoi University of Mining and Geology, Tu Liem, Hanoi, Vietnam*
[3]*Department of Chemistry and Biochemistry, National Chung Cheng University, Ming Hsiung, Chia Yi 621, Taiwan*
[4]*Institute of Materials Science, VAST of Vietnam, 18 Hoang Quoc Viet Road, Hanoi, Vietnam*
[5]*Graduate Institute of Opto-Mechatronics, National Chung Cheng University, Ming Hsiung, Chia Yi 621, Taiwan*
[6]*chelkc@ccu.edu.tw*
[7]*phyhck@ccu.edu.tw*
[*]*cchsu@phy.ccu.edu.tw*

Abstract: We present a novel type of surface-enhanced Raman scattering (SERS) substrate constituted of a 3-dimensinal polymeric inverse opal (IO) photonic crystal frame with gold nanorods (Au-NRs) decorating on the top layer. This substrate employs resonant excitation as well as constructive backward scattering of Raman signals to produce large enhancement of SERS output. For the incoming excitation, Au-NRs with appropriate aspect ratio were adopted to align their longitudinal localized surface plasmon band with the excitation laser wavelength. For the outgoing SERS signal, the spectral position of the photonic band gap was tuned to reflect Raman-scattered light constructively. This SERS substrate produces not only strong but also uniform SERS output due to the well control of Au-NRs distribution by the periodic IO structure, readily suitable for sensing applications.

OCIS codes: (160.5293) Photonic bandgap materials; (220.4241) Nanostructure fabrication; (240.6695) Surface-enhanced Raman scattering; (350.4238) Nanophotonics and photonic crystals.

References and links

1. K. Kneipp, M. Moskovits, and H. Kneipp, *Surface-enhanced Raman scattering: physics and applications* (Springer, 2006).
2. C. L. Haynes, A. D. McFarland, and R. P. Van Duyne, "Surface-enhanced Raman spectroscopy," Anal. Chem. **77**(17), 338A–346A (2005).
3. S. K. Saikin, Y. Chu, D. Rappoport, K. B. Crozier, and A. A. Aspuru-Guzik, "Separation of electromagnetic and chemical contributions to surface-enhanced Raman spectra on nanoengineered plasmonic substrates," J. Phys. Chem. Lett. **1**(18), 2740–2746 (2010).
4. A. D. McFarland, M. A. Young, J. A. Dieringer, and R. P. Van Duyne, "Wavelength-scanned surface-enhanced Raman excitation spectroscopy," J. Phys. Chem. B **109**(22), 11279–11285 (2005).
5. J. D. Driskell, R. J. Lipert, and M. D. Porter, "Labeled gold nanoparticles immobilized at smooth metallic substrates: systematic investigation of surface plasmon resonance and surface-enhanced Raman scattering," J. Phys. Chem. B **110**(35), 17444–17451 (2006).
6. A. Otto, "The "chemical" (electronic) contribution to surface-enhanced Raman scattering," J. Raman Spectrosc. **36**(6-7), 497–509 (2005).
7. M. Moskovits, "Surface-enhanced spectroscopy," Rev. Mod. Phys. **57**(3), 783–826 (1985).
8. M. Fleischmann, P. J. Hendra, and A. J. McQuillan, "Raman spectra of pyridine adsorbed at a silver electrode," Chem. Phys. Lett. **26**(2), 163–166 (1974).
9. D. L. Jeanmarie and R. P. Van Duyne, "Surface Raman spectroelectrochemistry, part 1: heterocyclic, aromatic, and aliphatic amines adsorbed on the anodized silver electrode," J. Electroanal. Chem. **84**, 1–20 (1977).

#178697 - $15.00 USD Received 25 Oct 2012; revised 26 Nov 2012; accepted 29 Nov 2012; published 17 Dec 2012

10. K. L. Kelly, E. Coronado, L. L. Zhao, and G. C. Schatz, "The optical properties of metal nanoparticles: the influence of size, shape, and dielectric environment," J. Phys. Chem. B **107**(3), 668–677 (2003).
11. C. J. Orendorff, L. Gearheart, N. R. Jana, and C. J. Murphy, "Aspect ratio dependence on surface enhanced Raman scattering using silver and gold nanorod substrates," Phys. Chem. Chem. Phys. **8**(1), 165–170 (2006).
12. P. F. Liao and A. Wokaun, "Lightning rod effect in surface enhanced Raman scattering," J. Chem. Phys. **76**(1), 751–752 (1982).
13. E. Hao and G. C. Schatz, "Electromagnetic fields around silver nanoparticles and dimers," J. Chem. Phys. **120**(1), 357–366 (2004).
14. J. Jiang, K. Bosnick, M. Maillard, and L. Brus, "Single molecule Raman spectroscopy at the junctions of large Ag nanocrystals," J. Phys. Chem. B **107**(37), 9964–9972 (2003).
15. M. Nikbakht and M. H. Mahdieh, "Optical responses of gold nanoparticles undergoing a change to cluster aggregates and laser beam characteristics effect," J. Phys. Chem. C **115**(5), 1561–1568 (2011).
16. C. Shi, L. Tian, L. Wu, and J. Zhu, "Layered aggregates of gold nanoparticles: solution and surface-assembled structures," J. Phys. Chem. C **111**(3), 1243–1247 (2007).
17. H. Xu, E. J. Bjerneld, M. Käll, and L. Börjesson, "Spectroscopy of single hemoglobin molecules by surface enhanced Raman scattering," Phys. Rev. Lett. **83**(21), 4357–4360 (1999).
18. C. Forestiere, A. J. Pasquale, A. Capretti, G. Miano, A. Tamburrino, S. Y. Lee, B. M. Reinhard, and L. Dal Negro, "Genetically engineered plasmonic nanoarrays," Nano Lett. **12**(4), 2037–2044 (2012).
19. J. J. Baumberg, T. A. Kelf, Y. Sugawara, S. Cintra, M. E. Abdelsalam, P. N. Bartlett, and A. E. Russell, "Angle-resolved surface-enhanced Raman scattering on metallic nanostructured plasmonic crystals," Nano Lett. **5**(11), 2262–2267 (2005).
20. A. Kocabas, G. Ertas, S. S. Senlik, and A. Aydinli, "Plasmonic band gap structures for surface-enhanced Raman scattering," Opt. Express **16**(17), 12469–12477 (2008).
21. F. H. Scholes, T. J. Davis, K. C. Vernon, D. Lau, S. A. Furman, and A. M. Glenn, "A hybrid substrate for surface-enhanced Raman scattering spectroscopy: coupling metal nanoparticles to strong localised fields on a micro-structured surface," J. Raman Spectrosc. **43**(2), 196–201 (2012).
22. H. H. Wang, C. Y. Liu, S. B. Wu, N. W. Liu, C. Y. Peng, T. H. Chan, C. F. Hsu, J. K. Wang, and Y. L. Wang, "Highly Raman-enhancing substrates based on silver nanoparticle arrays with tunable sub-10 nm gaps," Adv. Mater. (Deerfield Beach Fla.) **18**(4), 491–495 (2006).
23. H. Tang, G. Meng, Q. Huang, Z. Zhang, Z. Huang, and C. Zhu, "Arrays of cone-shaped ZnO nanorods decorated with Ag nanoparticles as 3D surface-enhanced Raman scattering substrates for rapid detection of trace polychlorinated biphenyls," Adv. Funct. Mater. **22**(1), 218–224 (2012).
24. C. Y. Wu, C. C. Huang, J. S. Jhang, A. C. Liu, C. C. Chiang, M. L. Hsieh, P. J. Huang, D. Tuyen, Q. Minh, T. S. Yang, L. K. Chau, H. C. Kan, and C. C. Hsu, "Hybrid surface-enhanced Raman scattering substrate from gold nanoparticle and photonic crystal: maneuverability and uniformity of Raman spectra," Opt. Express **17**(24), 21522–21529 (2009).
25. G. Frens, "Controlled nucleation for the regulation of the particle size in monodisperse gold suspensions," Nat. Phys. Sci (Lond.) **241**, 20–22 (1973).
26. L. D. Tuyen, C. Y. Wu, T. K. Anh, L. Q. Minh, H. C. Kan, and C. C. Hsu, "Fabrication and optical characterization of SiO_2 opal and SU-8 inverse opal photonic crystals," J. Exp. Nanosci. **7**(2), 198–204 (2012).
27. B. Nikoobakht and M. A. El-Sayed, "Preparation and growth mechanism of gold nanorods (NRs) using seed-mediated growth method," Chem. Mater. **15**(10), 1957–1962 (2003).
28. C. C. Huang, C. H. Huang, I. T. Kuo, L. K. Chau, and T. S. Yang, "Synthesis of silica-coated gold nanorod as Raman tags by modulating cetyltrimethylammonium bromide concentration," Colloids Surf. A Physicochem. Eng. Asp. **409**, 61–68 (2012).
29. R. Atkin, V. S. J. Craig, E. J. Wanless, and S. Biggs, "The influence of chain length and electrolyte on the adsorption kinetics of cationic surfactants at the silica-aqueous solution interface," J. Colloid Interface Sci. **266**(2), 236–244 (2003).
30. S. Link and M. A. El-Sayed, "Spectral properties and relaxation dynamics of surface plasmon electronic oscillations in gold and silver nanodots and nanorods," J. Phys. Chem. B **103**(40), 8410–8426 (1999).
31. J. Pérez-Juste, I. Pastoriza-Santos, L. M. Liz-Marzán, and P. Mulvaney, "Goldnanorods: synthesis, characterization and applications," Coord. Chem. Rev. **249**(17-18), 1870–1901 (2005).
32. S. Yun, Y. K. Park, S. K. Kim, and S. Park, "Linker-molecule-free gold nanorod layer-by-layer films for surface-enhanced Raman scattering," Anal. Chem. **79**(22), 8584–8589 (2007).
33. G. Wang, H. Y. Park, R. J. Lipert, and M. D. Porter, "Mixed monolayers on gold nanoparticle labels for multiplexed surface-enhanced Raman scattering based immunoassays," Anal. Chem. **81**(23), 9643–9650 (2009).
34. C. G. Blatchford, J. R. Campbell, and J. A. Creighton, "Plasma resonance – enhanced Raman scattering by adsorbates on gold colloids: the effects of aggregation," Surf. Sci. **120**(2), 435–455 (1982).
35. C. McLaughlin, D. Graham, and W. E. Smith, "Comparison of resonant and nonresonant conditions on the concentration dependence of surface enhanced Raman scattering from a dye adsorbed on silver colloid," J. Phys. Chem. B **106**(21), 5408–5412 (2002).

#178697 - $15.00 USD Received 25 Oct 2012; revised 26 Nov 2012; accepted 29 Nov 2012; published 17 Dec 2012

1. Introduction

Surface-enhanced Raman scattering (SERS) has been a subject of intensive research due to its potentials in many practical applications such as biological sensing and trace analysis [1,2]. SERS occurs to molecules adsorbed to roughened or nanostructured metal surfaces. It originates from two effects: the electromagnetic (EM) and the chemical (CM) enhancement mechanisms [1–7]. The EM mechanism is the direct result of enhancement of local EM field in the vicinity of a metal surface, due to its plasmonic response to an incident light [4,5]. The CM enhancement is attributed to resonant electronic charge transfer between adsorbed molecules and the metal surface, which increases the polarizability of adsorbed molecules and their Raman scattering cross section [3,6,7].

The key to promote the application of SERS is the development of substrates with large Raman signal enhancement and high reproducibility [7–9]. Noble metal nanoparticles, such as gold and silver nanoparticles on dielectric substrates have been shown highly effective for SERS application mainly due to the novelty of the localized surface plasmon resonance (LSPR) associated to these particles. The strength of LSPR is determined by the shape, size, inter-particle spacing, as well as the dielectric environment [2,10]. If the excitation wavelength aligns with the LSPR band, the SERS signal can be dramatically enhanced by the EM enhancement mechanism [4,5,11]. In addition, the lightning rod effect [12] with metal nanorods was estimated to be able to generate at least an order of magnitude stronger localized field than that of the isotropic plasmon band of metal nanospheres [13]. In practice, aggregation frequently occurs to metallic nanoparticles deposited on dielectric substrates. The cluster morphology generates uncontrolled hot-spot effect [14–17], making SERS signal inhomogeneous, thus limits its application. To produce high SERS intensity with good uniformity and reproducibility, many novel metallic nanostructures, including nanoparticle arrays, hollow structure films, grating structures, micro-structured surfaces, and 3-dimensinal (3D) hybrid substrates, etc., have been presented [18–23]. The search of cost-effective, high-sensitivity and high-reliability SERS substrates is still in progress.

Previously, we presented a hybrid SERS substrate based on a SU-8 inverse opal (IO) photonic crystal (PhC) decorated with gold nanospheres (Au-NSs) [24]. This hybrid SERS substrate produced uniform SERS signal due to the excellent control of the distribution of Au-NSs by the IO PhC [24]. Furthermore, in addition to the enhancement contributed from Au-NSs, a desired Raman signal can be selectively enhanced by appropriately overlapping the center of photonic band gap (PBG) of the IO PhC with the wavelength of the Raman signal. The PBG effect inhibits the Raman scattering photons transmitting through the IO PhC in the normal incident direction because the Bragg reflection caused by periodic multilayer structure. On the other hand, the PBG effect leads to a constructive interference of backward reflection Raman scattering light and results in strong enhancement of backward reflection Raman scattering signal [24]. Since no significant effort has been invested in resonating the LSPR of the Au nanoparticles (Au-NPs) with the excitation laser light, SERS signals generated from this hybrid SERS substrate were yet not fully optimized.

In this work, we investigated the advantages of incorporating gold nanorods (Au-NRs) onto SU-8 IO PhCs to further enhance SERS outputs. Au-NRs with appropriate aspect ratio were synthesized to have one of their LSPR bands aligned with the excitation laser wavelength. We compared SERS outputs from SU-8 IO PhC substrates decorated with Au-NRs and that with Au-NSs. The experimental results show that all Au-NRs decorated substrates produce higher SERS intensities, which is the direct evidence of resonant excitation of LSPR on Au-NRs. We also studied the effects of PhC structure on SERS output by comparing SERS intensities from Au-NRs decorated SU-8 IO substrates with different PBGs. It demonstrates that the PBG effect promotes the backward SERS output when the wavelength of the Raman signal aligns with the PBG. By careful designing structures of an Au-NRs decorated SU-8 IO PhC substrate, both resonant excitation of LSPR and PBG effects

#178697 - $15.00 USD Received 25 Oct 2012; revised 26 Nov 2012; accepted 29 Nov 2012; published 17 Dec 2012

can benefit simultaneously to selected Raman signals and leads to large enhancement of SERS signals.

2. Experiments

Au-NSs of 28 ± 4 nm were synthesized via the citrate reduction method, whose details can be found in the Ref [25]. and high-quality SU-8 IO PhCs were fabricated according to the experimental procedures described in previous work [26]. Au-NRs were synthesized according to the recipe reported by Nikoobakht and El-Sayed [27] with some modifications [28]. Firstly, the gold seed solution was prepared by mixing 5 ml of 0.5 mM $HAuCl_4.3H_2O$ with 5 ml of 0.2 M hexadecyltrimethylammonium bromide (CTAB, $C_{19}H_{42}BrN$, Acrôs), adding 0.6 µl of ice-cold solution of 0.01 M sodium borohydride ($NaBH_4$, Aldrich) and stirring for 2 min, which resulted in a solution with brownish yellow color. Subsequently, 300 µl of the seed solution was added to the growth solution which is a mixture of 50 ml of 0.2 M CTAB, 50 ml of 2.5 mM $HAuCl_4.3H_2O$, 1 ml of 4 mM silver nitrate ($AgNO_3$, Baker), and 2 ml of 0.788 M ascorbic acid ($C_6H_8O_6$, Sigma). The Au-NRs growth reaction was completed after 2 h, which was signaled by the color of the solution slowly changing from colorless to dark cyan. The temperature of both seed and growth solutions was kept at 24 °C.

Au-NRs were decorated on SU-8 planar and SU-8 IO substrates by a chemical modification process reported in Ref [24]. SU-8 surfaces were functionalized with SH group by immersing them in various aqueous solutions in the following sequence: 0.1 M sodium hydroxide (NaOH, Showa) for 1 h; 0.1 M potassium dichromate ($K_2Cr_2O_7$, Sigma) for 1 h; and a mixture of 0.43 mM of 1-ethyl-3-(3-dimethylaminopropyl)-carbodiimide ($C_8H_{17}N_3.HCl$, Sigma), 17 mM of N-hydroxysuccinimide ($C_4H_5NO_3$, Alfa Aesar), and 0.02 M of cystaminedihydrochloride ($C_4H_{12}N_2S_2.2HCl$, Alfa Aesar) for 2 h. To prepare the Au-NRs solution for decorating the SU-8 substrate, the concentration of CTAB in the Au-NRs solution was reduced by using centrifugation (8000 rpm) with deionized water twice. Finally, the SU-8 planar and SU-8 IO substrates were immersed in the Au-NRs solution, and 0.1 M sodium chloride (NaCl, Sigma) solution was subsequently added to the Au-NRs solution with volume ratio of NaCl:Au-NRs equal to 1:15. Due to the stable CTAB bilayer on Au-NRs, it is difficult to immobilize Au-NRs on thiol-terminated SU-8 surfaces. The addition of NaCl adjusted the ionic strength of the solution and, hence, the bilayer structure around the Au-NRs. It is noted that the addition of NaCl to the CTAB system resulted in a shift of the adsorption isotherm to lower surfactant concentration and an increase in maximal surface excess, leading to an increase in the rate of adsorption [29]. This has been attributed to electrostatic screening of head group charges and an increase level of counter-ion binding. Due to the hydrophobic property of SU-8 surface, ultrasonic treatment was applied for 2 min in each processing step to facilitate the reactions. All samples were cleaned by deionized water and blown dry with dry nitrogen after each step to avoid contamination. The average number density (σ) of Au-NRs increases monotonically with the immersion time, and the desired number density was obtained by controlling the immersion time in the final step. For comparison, we also prepared a glass substrate deposited with Au thin film of 30 nm thickness, and Au-NSs decorated SU-8 planar and SU-8 IO substrates with σ close to those of Au-NRs decorated substrates [24].

Prior to the SERS spectra measurement, all samples were immersed in an absolute ethanol solution (C_2H_5OH, Baker) containing 10^{-2} M of probe molecules 4-nitrobenzenethiol (4-NBT, $C_6H_5NO_2S$, Aldrich) for 2 min to allow the adsorption of 4-NBT molecules on the surface of Au-NPs. A He-Ne laser (Spectra Physics) with 20 mW output power at 632.8 nm wavelength was used to excite adsorbed 4-NBT molecules. A laser filter (Chroma Z633/10x) was used to remove other residual plasma lines from the incident beam. A 10x objective lens (NA = 0.25) was used to focus the laser beam onto the sample and also to collect back-scattered photons. A plano-convex lens was used to focus the scattered photons onto a fiber connected to a spectrometer (TRIAX 302, Jobin Yvon) equipped with a low temperature CCD detector. A

#178697 - $15.00 USD Received 25 Oct 2012; revised 26 Nov 2012; accepted 29 Nov 2012; published 17 Dec 2012

Raman filter (Omega XR3303) was used before the plano-convex lens to block the excitation laser. The integration time for each SERS spectrum was set to 15 s.

Transmission electron microscopy (TEM) (JEOL 2100) was used to determine the diameter of Au-NPs. Field emission scanning electron microscopy (FESEM) (Hitachi S4800) was used to characterize and inspect Au-NPs decorated on the SERS substrates. The PBG of SU-8 IO was determined via reflection spectrum measurement using a fiber optic spectrometer (Ocean S2000) with a halogen tungsten light source. Absorption spectra of Au-NPs solutions were measured using a UV-Vis spectrometer (Agilent).

3. Results and discussions

Figure 1(a) shows a FESEM image of Au-NRs decorated on a SU-8 planar substrate with σ = 60 μm^{-2}. The inset is a TEM image of Au-NRs with aspect ratio of 2.2 (length = 42 ± 5 nm, width = 19 ± 2 nm). Figures 1(b) and 1(c) show FESEM images of an Au-NRs decorated SU-8 IO substrate (lattice constant a = 466 nm) with σ = 65 μm^{-2}. As illustrated in Fig. 1(a) and 1(c), Au-NRs are uniformly distributed on the SU-8 planar substrate, while they appear more localized at the top grid regions of the SU-8 IO substrate. On both substrates, most Au-NRs are clearly separated, and only few Au-NRs are in close proximity of each other. After randomly checking different locations over a large area (1 x 1 cm^2), it is found that the Au-NRs distributions are similar to those shown in Figs. 1(a) and 1(c). For SU-8 planar substrates, the number density σ was obtained from FESEM images by directly counting the number of Au-NPs over a fixed area. For SU-8 IO substrates, since most nanoparticles are attached to the top layer and only few of them were found below the top layer, σ was determined by counting the number of Au-NPs visible on the top layer and divided by the area of the top grid and that of the spherical bottom visible in each void. Figure 1(d) shows the relation between σ of Au-NRs on a SU-8 IO PhC substrate and the immersion time in the final step of Au-NRs decoration. It is clear that σ increases monotonically with the immersion time. With this general trend, we are able to control σ of Au-NRs decorated on a SU-8 IO PhC substrate.

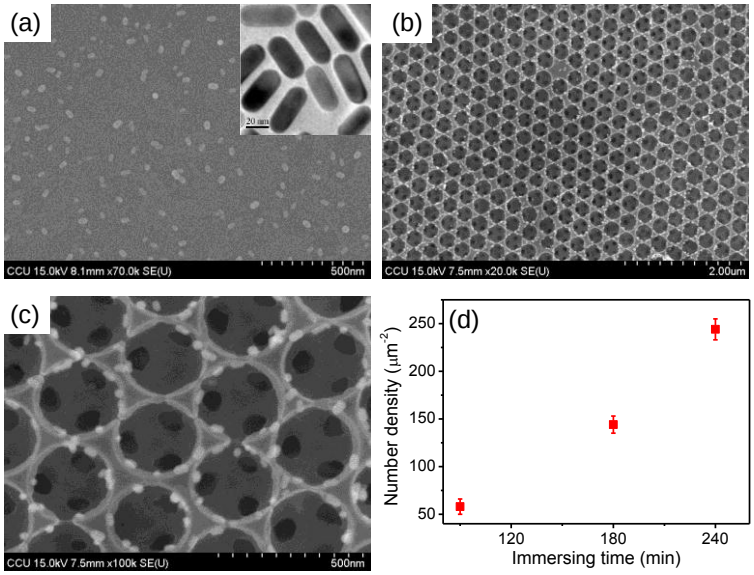

Fig. 1. (a) FESEM image of Au-NRs decorated on a SU-8 planar substrate with σ = 60 μm^{-2}. Inset: TEM image of Au-NRs.(b) and (c) FESEM images of Au-NRs decorated on a SU-8 IO substrate with σ = 65 μm^{-2}. (d) σ of Au-NRs on SU-8 IO substrates as a function of the immersion time.

#178697 - $15.00 USD Received 25 Oct 2012; revised 26 Nov 2012; accepted 29 Nov 2012; published 17 Dec 2012

To find plasmonic resonance of Au-NPs, their extinction spectra were measured before and after being decorated on SU-8 planar substrates. Figure 2 shows the extinction spectra of Au-NSs (black line) and Au-NRs (blue line) in aqueous solution. The spectrum of Au-NS solution contains a single absorption band centered at 523 nm, which corresponds to the plasmon absorption of Au-NSs. The spectrum of Au-NR solution exhibits two distinct absorption bands with one centered at 518 and the other at 645 nm, and they are attributed to the transverse and longitudinal surface plasmon modes of Au-NRs, respectively [30]. The extinction spectra of Au-NSs ($\sigma \approx 272\ \mu m^{-2}$, red line) and Au-NRs ($\sigma \approx 245\ \mu m^{-2}$, cyan line) on SU-8 planar substrates are also shown in Fig. 2. The peak position of Au-NSs spectrum is at 524 nm, and the peak positions of transverse and longitudinal surface plasmon absorptions of Au-NRs are at 519 and 636 nm, respectively. In general, their spectral profiles and peak positions are almost identical to those of the aqueous solutions, except there is a small blue-shift of the longitudinal surface plasmon resonance of Au-NRs, probably due to the change of environment from aqueous solution to air [31]. In addition, even increasing σ of Au-NPs on the SU-8 planar substrate up to ~$450\ \mu m^{-2}$, we found that the positions and widths of plasmon absorption peaks remain unchanged. This indicates that Au-NPs were well separated on the substrate; unlike the previous result of multilayer thin films composed of Au-NPs, whose extinction spectra exhibited significant difference to those of aqueous solution because of the aggregation of the nanoparticles [16,32]. Since the longitudinal surface plasmon absorption of Au-NRs matches well to the excitation by He-Ne laser irradiation at 632.8 nm, we expect strong localized EM fields can be built-up in the vicinity of surfaces of Au-NRs due to resonantly excited localized surface plasmon on NRs.

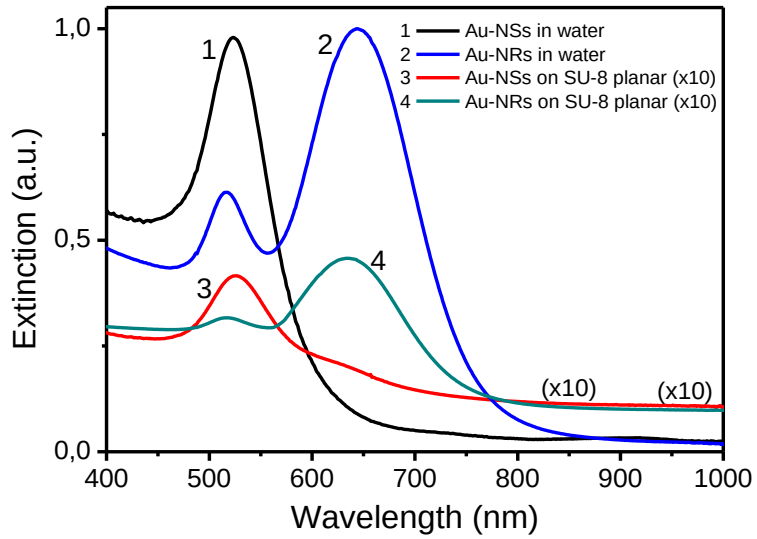

Fig. 2. UV-Vis extinction spectra of Au-NSs and Au-NRs in aqueous solution and deposited on SU-8 planar substrates. For clarity, the vertical values corresponding to curve 3 and 4 were multiplied by a factor of 10. The average diameter of Au-NSs is 28 ± 4 nm. The average length and width of Au-NRs are 42 ± 5 nm and 19 ± 2 nm, respectively. The number densities σ are 272 and 245 μm^{-2} for Au-NSs and Au-NRs decorated on SU-8 planar substrates, respectively.

To investigate the effect of resonance excitation of LSPR of Au-NPs and the effect of PBG on the SERS output, we fabricated SU-8 IO PhC substrates with different lattice constants decorated with both types of Au-NPs. Major samples used for detailed comparison in this study are listed in Table 1.

#178697 - $15.00 USD Received 25 Oct 2012; revised 26 Nov 2012; accepted 29 Nov 2012; published 17 Dec 2012

Table 1. Au-NPs decorated SU-8 substrates*

Label	Substrate	Particle type	σ(μm-2)
A	SU-8 IO, a = 424 nm, λ_{PBG} = 573 nm	Au-NR	62
B	SU-8 IO, a = 466 nm, λ_{PBG} = 628 nm	Au-NR	65
C	SU-8 IO, a = 509 nm, λ_{PBG} = 686 nm	Au-NR	50
D	SU-8 IO, a = 559 nm, λ_{PBG} = 745 nm	Au-NR	55
E	SU-8 IO, a = 608 nm, λ_{PBG} = 812 nm	Au-NR	58
F	SU-8 Planar surface	Au-NR	60
G	SU-8 IO, a = 466 nm, λ_{PBG} = 626 nm	Au-NS	78
H	SU-8 IO, a = 509 nm, λ_{PBG} = 688 nm	Au-NS	82
I	SU-8 Planar surface	Au-NS	72
J	SU-8 Planar surface	Au film	N/A

*a is the lattice constant of the IO structure, and λ_{PBG} the peak wavelength of the reflection spectrum of the IO structure measured at normal incidence, σ is the average number density of the Au-NPs decorated on the substrate.

Figure 3 shows the reflection spectra measured at normal incidence from sample A to E. The PBG reflection peak wavelength shifts from 573 to 812 nm as the lattice constant increases from 424 to 608 nm, with the full width at half maximum (FWHM) of their reflection peak equal to 56, 59, 61, 65, and 72 nm, respectively. The increase of σ up to ~250 μm^{-2} red-shifted the peak positions by about 2 nm, but made no change in FWHM of the peaks. Note that the reflection spectra of SU-8 IO substrates did not change after the adsorption of 4-NBT probe molecules. That is because most Au-NRs are decorated only on the top layer of SU-8 IO substrates, and the adsorption of 4-NBT probe molecules is insignificant to change the effective refractive index inside the IO PhC.

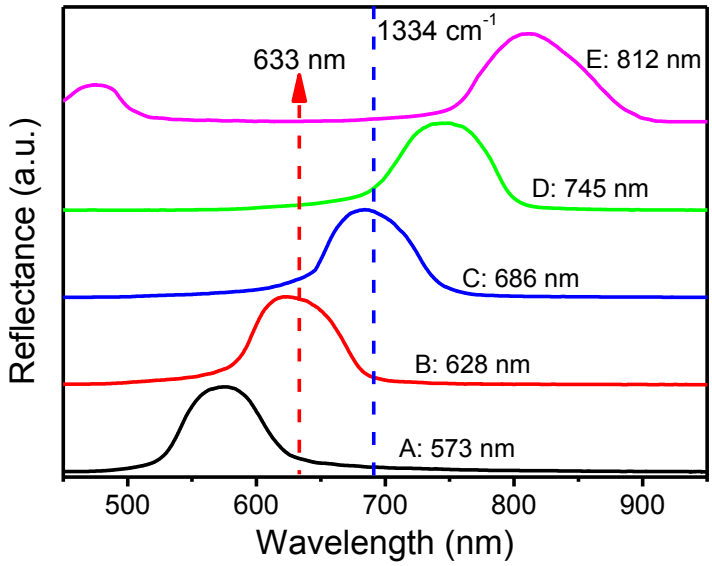

Fig. 3. Normal-incident reflection spectra of Au-NRs SU-8 IO substrates. The dashed lines denote wavelengths of excitation laser at 632.8 nm and the Raman-shifted peak at 1334 cm^{-1} (691 nm) of 4-NBT molecules.

To investigate PBG and the plasmon resonance excitation effects on SERS output, we measured SERS spectra of 4-NBT probe molecules adsorbed onto the substrates in Table 1. Figure 4(a) compares their SERS outputs, where the spectral features agree well with previous reported results [24,33]. For ease of comparison, each curve is shifted vertically by an appropriate height and the order of the spectra is arranged according to the strength of SERS intensity from top to bottom. Figure 4(b) shows peak intensities of Raman peak at 1334 cm^{-1} (λ = 691 nm) in Fig. 4(a) from substrate A to J. To see the effect of resonant excitation of

#178697 - $15.00 USD Received 25 Oct 2012; revised 26 Nov 2012; accepted 29 Nov 2012; published 17 Dec 2012

LSPR on Au NPs, we first compare the SERS intensity from planar SU-8 substrates with Au-NRs, Au-NSs, and Au film on top, i.e. samples F, I, and J, respectively. Sample F produced the strongest Raman sensitivity, and sample J the weakest. This result indicates that the matching of the longitudinal plasmon absorption band of Au-NRs with the excitation laser wavelength resulted in the largest Raman output among these three samples (see Fig. 2), in agreement with the expectation of stronger EM field built up in the vicinity of Au-NRs [11]. This trend is also true for IO substrates in general by comparing the SERS intensities from sample A to E to those from sample G and H. More specifically, comparing the Raman intensities from IO substrates with nearly the same λ_{PBG}, namely samples B and G, (and samples C and H as well), the Au-NRs decorated SU-8 IO substrates (samples B and C) produced SERS intensity about 5 to 5.5 times higher than their Au-NSs decorated counterpart (samples G and H) did, because of the well matching of the longitudinal plasmon absorption band of Au-NRs with the excitation laser wavelength. Above results clearly demonstrate the role of resonant excitation of LPSR on Au-NRs in SERS signal enhancement.

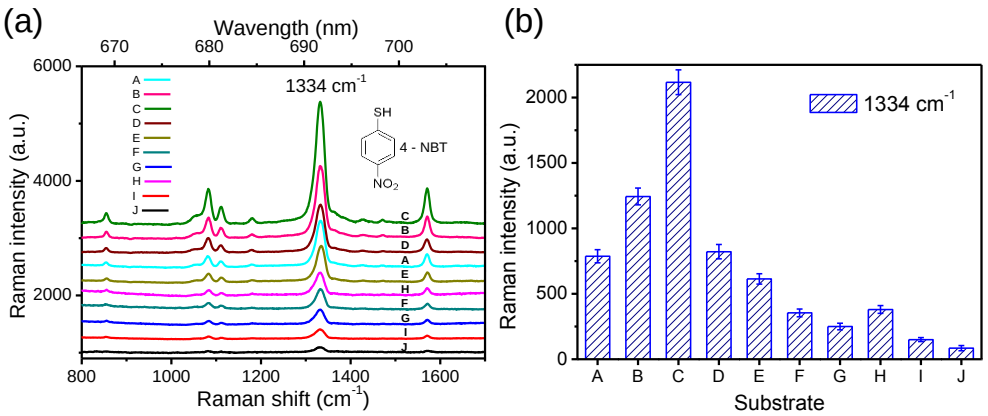

Fig. 4. (a) SERS spectra of 4-NBT molecules adsorbed on SERS substrates listed in Table 1. The curves are arranged according to their SERS intensities from top to bottom. The inset shows the molecular structure of 4-NBT. (b) SERS intensities of the major Raman peak 1334 cm^{-1} (λ = 691 nm) of 4-NBT probe molecules obtained from substrates A to J.

For the PBG effect, we compare the SERS intensities from sample A to F. As shown in Fig. 4(b), the order of the Raman intensities generated from these samples from high to low are: $I_C >> I_B > I_D \approx I_A > I_E > I_F$. Sample C produced the highest Raman intensity because the Raman-shifted wavelength aligns with its PBG (see Fig. 3). The PBG effect prohibits the transmission of Raman-shifted photons scattered by 4-NBT molecules adsorbed on Au-NRs in the normal incident direction, which were deposited only on the top layer of the SU-8 IO substrate. Constructive interference of the backward reflection of Raman scattering photons leads to further enhancement. Similar effect can also be seen from Au-NSs decorated SU-8 IO substrates [24]; the SERS intensity generated from sample H was larger than that of G for the same reason.

As displayed in Fig. 3, the excitation laser wavelength aligns with the PBG of sample B, and accordingly results in high reflection of the excitation light, thus strong interaction between excitation light and Au-NRs, which only existed on the top layer of the SU-8 IO substrate. This presumably should also enhance the EM field around probe molecules and therefore increases the Raman scattering intensity. Nevertheless, this kind of enhancement effect is still smaller than that from aligning the Raman-shifted wavelength with the PBG of the IO substrate. For samples A, D, and E, the Raman intensities decrease with the spectral gap between PBG of the substrate and wavelength of either the Raman-shifted peak or the excitation laser wavelength. To the extent that when both the Raman-shifted peak and the

#178697 - $15.00 USD Received 25 Oct 2012; revised 26 Nov 2012; accepted 29 Nov 2012; published 17 Dec 2012

excitation laser wavelengths were far away from the PBG (sample E), the PBG had no effect in enhancing the Raman signal and thus produced the smallest SERS intensity among the Au-NRs decorated SU-8 IO substrates.

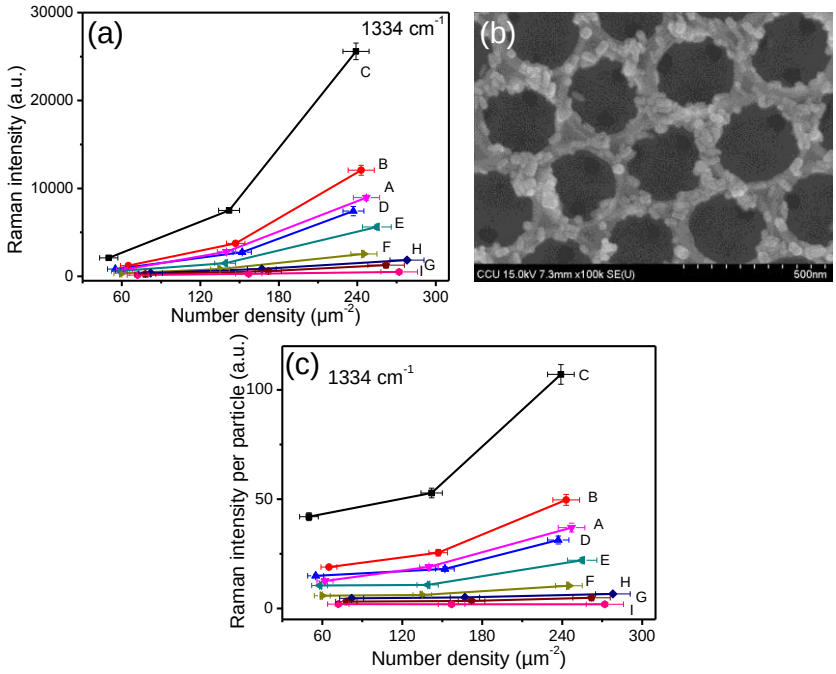

Fig. 5. (a) Au-NR number density (σ) dependence of SERS intensities of the Raman peak at 1334 cm^{-1} (691 nm) of 4-NBT probe molecules measured from substrate A to I. The sample specification in Table 1 applies to the alphabetic labeling here except the number density of Au-NRs. (b)The FESEM image of Au-NRs decorated on a SU-8 IO substrate with σ = 243μm^{-2}. (c) The σ dependence of the same signal in (a) normalized with σ.

Raman spectroscopy is concentration dependent, but "hot-spot" effect often causes the concentration dependency to deviate from linearity [34,35]. Hence, we further explore the dependence of the SERS signal on the number density σ of NPs decorated on the substrate. Figure 5(a) shows SERS intensities of the peak at 1334 cm^{-1} as a function of σ for substrates A to I. As expected, the Raman intensities increase with σ, but a nonlinear growth of Raman intensities can be clearly seen in plots for substrates A to E. From the FESEM images of substrates A to E with high σ, aggregates of Au-NRs typically exist in most top grid regions (see Fig. 5(b)),which likely results in the hot-spot effect. We normalized the signal intensities in Fig. 5(a) with σ and plotted the results in Fig. 5(c). It is clear when σ increases, the average of SERS intensities at 1334 cm^{-1} of each nanoparticle remains constant for substrate F to I, which represents hot-spot effect is absent. On the other hand, the Raman intensities of each Au-NR of substrates A to E exhibit substantial increase as σ exceeds 145 μm^{-2}. This indicates that hot-spot effect has strong impact on the SERS outputs of substrates A to E for σ > 145μm^{-2}, but it is insignificant for σ ≤ 145μm^{-2}. This indicates that hot-spot effect is insignificant to the SERS outputs of the substrates decorated with low σ (for example, σ ≈50 μm^{-2}) of Au-NRs or Au-NSs. We further found that even with hot-spot effect present the Au-NRs decorated SU-8 IO substrates still produce spatially uniform SERS signal. The SERS signal from substrate C with σ = 239 μm^{-2} were measured at 10 different positions within an area of 1 x 1 cm^2. The standard deviation of the SERS signal was found to be only 5%,

#178697 - $15.00 USD Received 25 Oct 2012; revised 26 Nov 2012; accepted 29 Nov 2012; published 17 Dec 2012

indicating SU-8 IO substrates provide excellent control of the distribution of Au-NRs that produces highly uniform SERS outputs.

4. Conclusions

In this work, a novel type of PhC SERS substrate is presented for producing large enhancement of SERS output. The proposed SERS substrate contains a 3D SU-8 IO PhC backbone and its top layer is decorated with appropriate aspect ratio of Au-NRs. We demonstrate that Au-NRs can promote the excitation of LSPR and increase SERS output. In addition, we also show that the backward SERS output of a SU-8 IO PhC substrate can be enhanced via PBG effect. The PBG effect takes place as the Raman-shifted wavelength of probe molecules aligns with the PBG. Combining these two effects, strong SERS output with high spatial uniformity can be generated. The novel type SERS substrate should be useful for sensing applications.

Acknowledgments

The authors gratefully acknowledge the financial support from the National Science Council (NSC), Taiwan, under grant Nos. NSC 98-2112-M-194-008-MY3, NSC 99-2112-M-194-008-MY3, NSC 98-2811-M-194-007, and NSC 99-2113-M-194-001-MY3. L. D. Tuyen acknowledges the support of Taiwan Scholarship from NSC, Taiwan. L. Q. Minh and L. D. Tuyen acknowledge the support of Vietnam-NAFOSTED foundation, under grant No. 103.06.46.09.

#178697 - $15.00 USD Received 25 Oct 2012; revised 26 Nov 2012; accepted 29 Nov 2012; published 17 Dec 2012